Biointerface Research in Applied Chemistry
Platinum Open Access Journal (ISSN: 2069-5837)

Article
Volume 12, Issue 3, 2022, 3996 - 4017
https://doi.org/10.33263/BRIAC123.39964017

Vibrational Spectral Studies, Quantum Mechanical Properties, and Biological Activity Prediction and Inclusion Molecular Self-Assembly Formation of N-N'-Dimethylethylene Urea

Sushma Priya Yeddu [1], Pooventhiran Thangaiyan [2], Adamilli Veeraiah [3], Dharmarpu Vijay [3], Katta Eswar Srikanth [3], Ahmad Irfan [4,5], Renjith Thomas [2,*]

1 Department of Physics, Adikavi Nannaya University, Rajamahendravaram, Andhra Pradesh, India
2 Department of Chemistry, St Berchmans College (Autonomous), Changanassery, Kerala, India; pooventhiran134@gmail.com (T.P.);
3 Molecular Spectroscopy Laboratory, Department of Physics, DNR College (A), Bhimavaram, A.P., India
4 Research Center for Advanced Materials Science (RCAMS), King Khalid University, P.O. Box 9004, Abha 61413, Saudi Arabia
5 Department of Chemistry, Faculty of Science, King Khalid University, P.O. Box 9004, Abha 61413, Saudi Arabia
* Correspondence: renjith@sbcollege.ac.in (R.T.);

Scopus Author ID 55481779800
Received: 2.03.2021; Revised: 15.05.2021; Accepted: 18.05.2021; Published: 13.08.2021

Abstract: A cyclic urea analog, N-N'-dimethylethylene urea, was studied using different spectral methods like FT-IR, FT-Raman, and UV-VIS methods followed by computational simulations. The experimental and simulated spectra are compared, and a detailed assignment of vibrations and potential energy distribution is made. It was followed by various quantum mechanical studies like frontier orbital analysis, energy descriptors, average local ionization energies, and nonlinear optical properties. The NBO gave an insight into the various intramolecular stabilizing electron delocalization by hyperconjugation. Noncovalent interaction analysis provided various types of interactions present in the molecule. We also studied ALIE, local information entropy, electron localized function, reduced density gradient studies, localized orbital locator studies, and other analyses. Molecular docking results indicated that this urea derivative acted as an ATP-hydrolysing inhibitor, and the drug delivery ability of cyclodextrin on NND was tested by forming an inclusion complex with both compounds with dispersion and without dispersion interaction.

Keywords: DFT; NND; ALIE; NCI; drug delivery.

1. Introduction

Heterocyclic compounds of nitrogen are of significant importance in biology and chemistry due to their prolific uses in the pharmaceutical industry. Among them, cyclic urea-type analogs are found to show a variety of applications in different fields, especially in the medicinal and agricultural disciplines [1]. Disubstituted urea has ample therapeutic activities, for instance, potent inhibitors of different parasites like worms, plasmodium, HIV, diuretic activity, pain-relieving properties, activity against bacteria, algae, and fungi [2–5]. N, N′-disubstituted urea derivatives can effectively control and inhibit soluble epoxide hydrolase, both *in vivo* and *in vitro*. They are also used to treat Raynaud disease, respiratory distress, high

blood pressure, complications arising from diabetics, rheumatoid arthritis, and kidney complications [6].

This manuscript presents the detailed experimental and computational study of structure, spectra, and applications of a simple heterocyclic urea derivative N-N'-dimethylethylene urea (NND). Shababan discussed the structure and the IR spectrum of this compound, but it lacks the detailed study of the electronic properties, molecular properties, reactivity descriptors, biological studies, drug delivery properties, and other basic studies [7]. Hence we decided to pursue this molecule in detail for its structure, electronic properties, physicochemical properties, noncovalent interactions, and potential biological activities using experimental and computational methods [8–15]. We have used various spectral methods like IR, UV, and Raman to investigate the compound's structural features. The biological activity was also predicted using the PASS study and found that it is active as an inhibitor of ATP hydrolysis. Being a drug, drug delivery is also important. We tried whether this compound can be used along with cyclodextrin by forming a molecular inclusion compound and simulated the complex with and without dispersion [16–21].

2. Materials and Methods

The compound was purchased from Sigma Aldrich and used as such for all the experimental studies. The compound's FT-IR and FT Raman spectra were recorded using a Nicolet FT-IR spectrometer and a Nicolet Magna Raman spectrometer equipped with Nd: YAG laser source and InGaAs detector, respectively. UV-Vis spectrum was recorded using Specord Spectrometer at room temperature with DMSO as the solvent.

The first step in the computational section is optimizing the molecule using Gaussian 09 software [22]. We optimized the molecule using the DFT formalism with B3LYP functional [23–27]and 6-311++G (d,p) basis set [28–32]. The same level is used for generating IR and Raman spectra of the compounds. Frequency calculations ensured that there are no imaginary frequencies in the simulated spectrum such that it corresponds to a global minimum. The scaled IR and Raman frequencies are compared with experimental values and found in close agreement. Detailed potential energy distribution and vibration assignments were performed for the compound. The NBO computations were carried out with NBO 3.1 program [33]. Gauss Sum [34] software was employed to study the calculated spectra. Reaction sites of NND were calculated using Multiwavefunction [35] software for calculating total electrostatic potential, average localized ionization energy, and noncovalent interactions. NND biological activity received from PASS online [36] the site, suitable PDB ID downloaded from RCSB [37] site, the energy received from SwissDock [37]and the score values received from PatchDock [38,39] and docked results collected from bio-discovery studio [40] software.

3. Results and Discussion

3.1. IR and RAMAN spectra.

The molecule was optimized to a minimum conformation using DFT with B3LYP functional and 6-311+G(d,p) basis set and is given in Figure 1. The presence of no imaginary frequencies ensured that we got a minimum energy geometry. The generated scaled IR and Raman spectra using the same theoretical level were compared with the experimental obtained FT-IR and FT-Raman spectrum and found in close agreement. From the local symmetry coordinates with appropriate scale factors (supplementary material Table S1), the vibrational

assignments are made according to the PED matrix (Table 1). The comparative FT-IR and FT-Raman spectra are shown in Figure 2 and Figure 3.

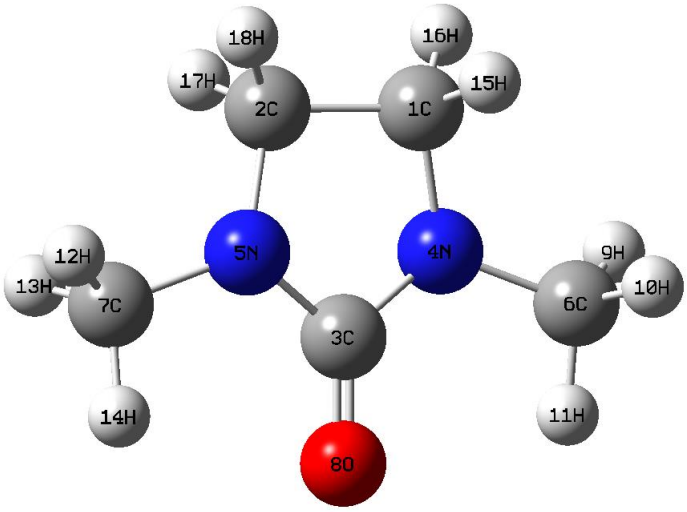

Figure 1. Optimized geometry structure of N-N'-dimethylethyleneurea.

Table 1. Detailed assignments of fundamental vibrations of N-N'-dimethylethylene urea by normal mode analysis based on SQM force field calculations using B3LYP/6-311++G(d,p).

Mode no.	FT-IR		Activity		Assignments (PED) [a, b]
	Experimental frequencies (cm^{-1})	Theoretical frequencies (cm^{-1})	IR	RAMAN	
7	3272 v	3134	1.970	102.70	υ CH3op (98)
8		3133	34.109	6.922	υ CH3op (98)
9		3072	61.341	98.607	υ CH2as (48)
10	3059 vs	3059	10.439	72.427	υ CH2as (46)
11		3044	60.865	36.565	υ CH3ip (98)
12		2965	7.507	129.916	υ CH3ip (98)
13	2935 vs	2935	75.638	206.876	υ CH2ss (91)
14	2857 s	2860	57.379	24.619	υ CH2ss (94)
15		2460	0.065	287.464	υ CH3ss (99)
16	2459 vs	2459	138.460	0.211	υ CH3ss (99)
17		1770	19.063	15.609	β CH3ib (79), β CH3ob (20)
18	1687 vs	1687	0.123	17.364	β CH3ib (69), β CH3ob (15)
19	1500 s	1528	266.570	6.696	υ CN (43), υ CO (20)
20		1513	300.510	1.846	υ CN (57)
21		1456	35.716	5.945	β CH2sc (62), β CH2tw (26)
22	1436 s	1435	14.549	10.245	β CH2sc (80)
23		1425	0.138	13.686	β CH2tw (57), β CH2sc (31)
24		1408	10.103	5.130	υ CN (37), β CH3sb (33)
25		1400	9.416	10.492	β CH3sb (53), β CH2tw (21)
26	1397 s	1395	38.396	4.135	β CH3sb (38), β CH2tw (34), υ CN (19)
27		1389	57.629	3.002	β CH3sb (44), υ CN (24), β Rsym (16)
28		1343	37.803	4.308	υ CN (30), β CH2tw (28), β CH3or (18)
29		1312	58.702	6.080	β CH3or (24), υ CN (24), υ CO (20)
30	1274 s	1266	101.93	1.520	β CH2wa (66), υ CN (21)
31	1242 w	1254	1.756	26.311	β CH2wa (39), β CH3or (26)
32	1203 s	1194	56.618	0.842	υ CN (43), β CH3or (33), β CH3ob (15)
33		1152	0.464	7.155	β CH3ir (47)
34		1132	3.384	6.802	β CH3ir (46), β CH3ob (24), β CH3ib (18)
35	1076 vw	1091	4.312	12.199	β CH3ob (38), υ CN (19), β CH3ib (18)
36		1060	0.912	1.629	β CH2ro (56), β CH3ob (17)
37	1024 w	1037	6.309	8.185	β CH3ob (48), β CH3ib (21), υ CN (15)

Mode no.	FT-IR		Activity		Assignments (PED) [a, b]
	Experimental frequencies (cm^{-1})	Theoretical frequencies (cm^{-1})	IR	RAMAN	
38		994	13.891	4.036	β CH3ob (53), β CH3ib (22)
39	985 vs	972	2.306	3.232	β CH3ob (57), β CH3ib (24)
40	961 vs	952	13.873	6.192	β CH3ob (44), β CH3ib (19), υ CC (17)
41	858 s	855	6.658	0.934	β CH2ro (64)
42	759 vs	759	20.811	0.971	ω CO (67), τ Rsym (21)
43		730	19.431	20.405	υ CN (63), υ CO (29)
44	648 w	652	8.003	3.016	β Rasy (41)
45	581 s	577	18.084	2.030	β Rsym (51), υ CN (28)
46		521	5.546	0.889	β NCO (34), υ CN (25), β NC (19)
47		322	13.513	1.404	β NC (63), β NCO (19)
48		272	0.405	0.013	β NC (70)
49		262	2.151	0.902	ω CN (43), τ Rasy (36)
50		220	8.769	0.495	τ Rsym (48), ω CN (36)
51		187	0.008	0.369	ω CN (51), τ Rasy (28)
52		165	1.676	0.563	τ NCH3 (63), τ Rsym (22)
53		159	0.005	0.842	τ NCH3 (67), τ Rasy (15)
54		113	8.543	0.130	ω CN (78)

a Only PED contributions ≥15% are listed by DFT method. (RMS FREQUENCY ERROR: 0.832E+01)

b Abbreviations: υ, stretching; β, in-plane bending; ω, out of plane bending; τ, torsion, ss, symmetrical stretching, as, asymmetrical stretching, sc, scissoring, wa, wagging, twi, twisting, ro, rocking, ipb, in-plane bending, opb, out-of-plane bending; tri, trigonal deformation, sym, symmetrical deformation, asy, asymmetric deformation, butter, butterfly, ar, aromatic, sub, substitution, vs, very strong; s, strong; ms, medium strong; w, weak; vw, very weak.

For the compound, υ CH3 op vibrations are assigned at 3272 cm^{-1} (IR) and at 3134 cm^{-1} theoretically υ CH3 symmetric stretching vibrations are allocated at 2459 cm^{-1} (IR) and theoretically at 2459 cm^{-1}. β CH3 vibrations are observed at 1687,1436,1397,1076,985,961 cm^{-1} (IR) and theoretically from 1770-952 cm^{-1} region.

υ CH2 symmetric stretching vibrations are allocated at 2459 cm^{-1} (IR) and theoretically at 2459 cm^{-1}. υ CH2as vibrations are allocated at 3059 cm^{-1} (IR and Raman) and theoretically at 3059 cm^{-1}. β CH2sc, CH2wa, CH2tw , CH2ro, vibrations are observed at 1436, 1397, 1274, 858 cm^{-1} and 1435, 1395 ,1266, 855 cm^{-1} using DFT.

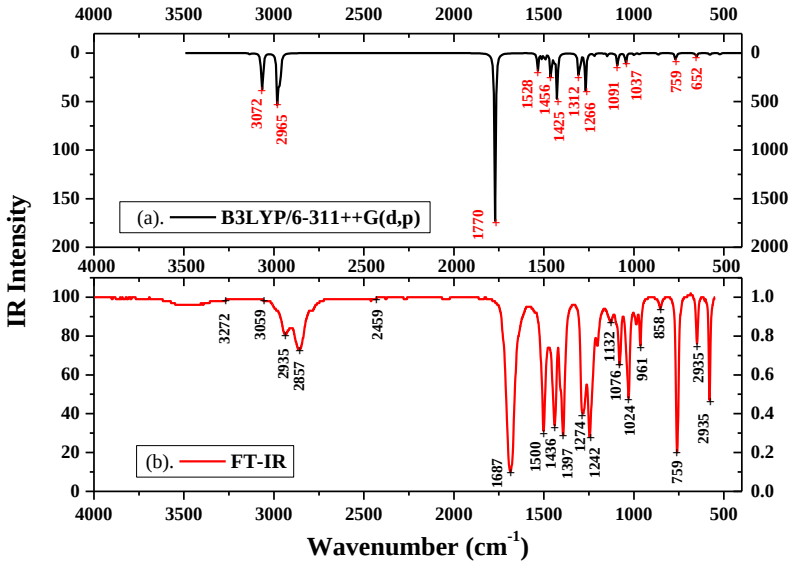

Figure 2. FT-IR experimental and simulated spectrum of N-N'-dimethylethyleneurea.

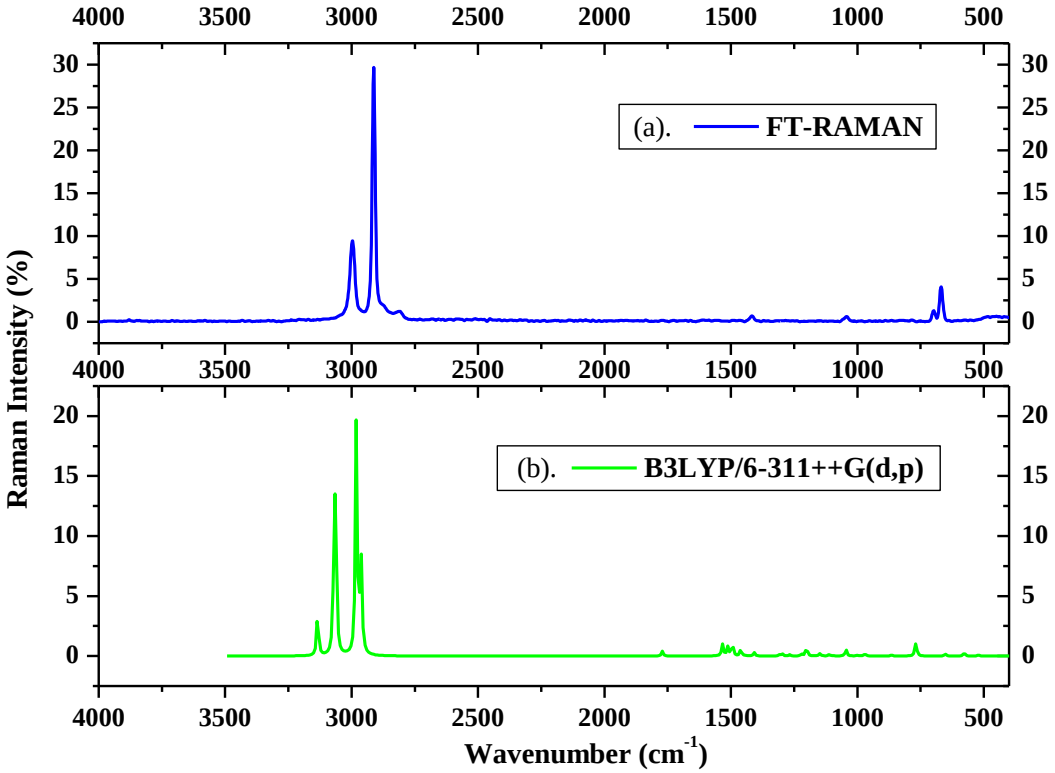

Figure 3. FT-Raman experimental and simulated spectrum of N-N'-dimethylethyleneurea.

The assignment of CN vibrations is a difficult task since the mixing of vibrations occurs in this region. υ CN vibrations are observed at 1500 cm^{-1} (IR) and by DFT calculations at 1528 $cm^{-1,}$ and β NC vibrations are observed theoretically at 322 cm^{-1}. ω CO vibrations are measured at 759 cm^{-1}(IR) and through DFT at 759 cm^{-1}. Ring Symmetric and antisymmetric vibrations are observed at 581, 648 cm^{-1} (IR) and theoretically at 577, 642 cm^{-1}. The observed and calculated wavenumbers show good coincidence.

3.2. UV-visible spectrum.

The Experimental UV-visible spectrum of the title compound is shown in figure 4. The maximum absorption peak is observed at 256.50 nm. The peak suggests that the absorption is due to electron transition from n-π*, which is the only transition for the C=O bond. Moreover, the observed shift is due to the presence of auxochrome together with the interaction of solvent DMSO. The UV–Vis excitation wavelength and absorbance of the compound are shown in Table 2.

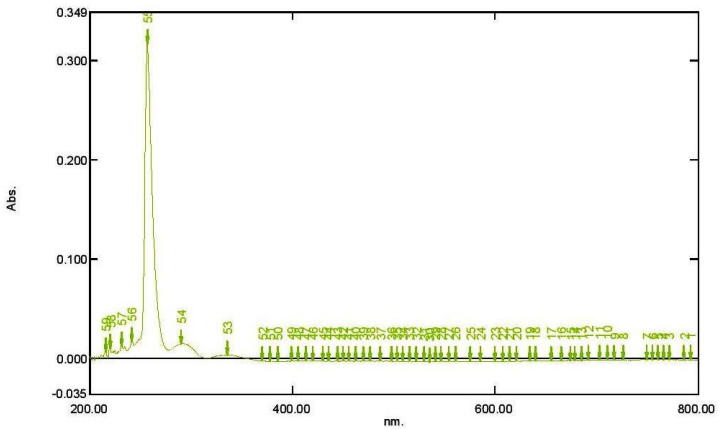

Figure 4. Experimental UV-Vis spectrum of N-N'-dimethylethylene urea.

Table 2. Experimental UV data of N-N'-dimethylethylene urea.

Wavelength	Absorbance
336	0.004
314.5	0.001
290.5	0.015
278	0.009
256.5	0.317
243.5	0.014
241.5	0.018
236.5	0.008
231.5	0.013
226.5	0.005
219.5	0.011
217.5	0
215.5	0.007

3.3. Frontier molecular orbitals of NND.

The HOMO-LUMO graph is shown in Figure 6, and HOMO is delocalized over the molecule, whereas LUMO is localized over the methylene group of the phenyl ring. The calculated HOMO and LUMO energies, ionization potential ($I=-E_{HOMO}$), electron affinity($A=-E_{LUMO}$), and HOMO-LUMO energy gap were computed as 6.4651, 0.4059, and -6.0591 eV, which shows the reactivity of the compound with less energy gap. Moreover, the quantum mechanical parameters such as chemical hardness η= (I-A)/2=6.2621, chemical potential μ=-(I+A)/2=3.4355 and Electrofilicity index $\omega = \frac{\rho^2}{2\eta} = 0.9424$ and other essential parameters were calculated and tabulated in Table 3.

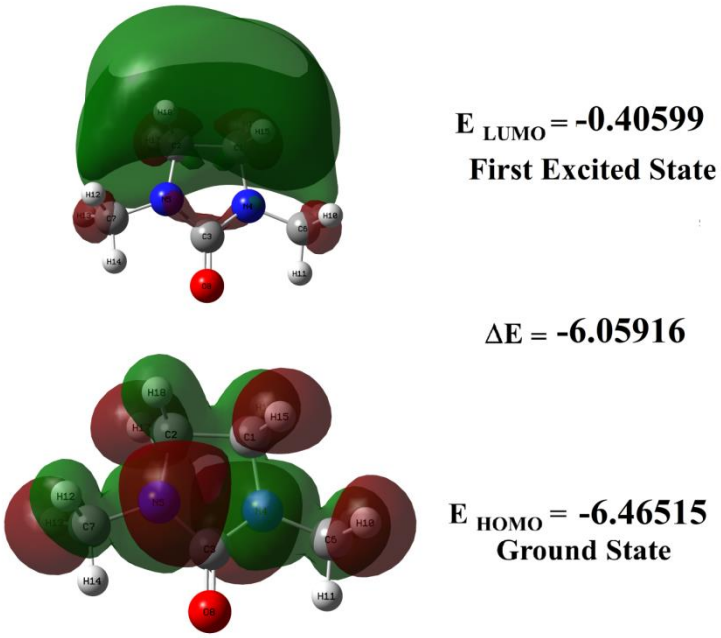

Figure 5. Ground-state (HOMO: 31) and First exited state (LUMO: 32) representation.

Table 3. The calculated quantum chemical parameters of N-N'-dimethylethylene urea.

Property	NND
Total energy (eV)	-10378.7347
E_{HOMO} (eV)	-6.4651
E_{LUMO} (eV)	-0.4059
Energy gap (ΔE) (eV)	-6.0591
Ionization potential (I) eV	6.4651

Property	NND
Electron Affinity (A) eV	0.4059
Electro-negativity (χ)eV	6.6681
Chemical Potential (μ)	3.4355
Chemical hardness(η)eV	6.2621
Electrofilicity index (ω)eV	0.9424
Global Softness (σ)eV	0.1596
Dipole moment(D)	4.1069

3.4. NBO analysis and NLO properties.

The interaction between the lone pair orbitals and bonded orbitals causes the stabilization of the molecule. These interactions can be well studied using the concept of natural bond orbitals. NBO calculations have been implemented in the Gaussian suite, and the data obtained helps to understand the delocalization of electrons and hyperconjugation [41,42].

Table 4. Second order perturbation theory analysis of fock matrix in NBO basis for N-N'-dimethylethylene urea.

Donor(i)	Type	Ed/e	Acceptor(j)	Type	Ed/e	$E^{(2)a}$ (kJ mol^{-1})	E(i)-E(j)[b] (a.u)	f(i,j)[c] (a.u)
C1-C2	Σ	1.9779	N4-C6	σ*	0.0152	4.04	0.98	0.056
	Σ		N5-C7	σ*	0.0152	4.04	0.98	0.056
C1-N4	Σ	1.9827	C2-N5	σ*	0.0204	1.19	1.07	0.032
	Σ		C3-O8	π*	0.0119	4.24	1.36	0.068
C1-H15	Σ	1.9858	C2-H17	σ*	0.0296	1.96	0.90	0.038
C1-H16	Σ	1.9858	C3-N4	σ*	0.0844	1.98	0.97	0.040
C2-N5	Σ	1.9827	C1-N4	σ*	0.0204	1.19	1.07	0.032
	Σ		C3-O8	π*	0.0119	4.24	1.36	0.068
C2-H17	Σ	1.9858	C1-H15	σ*	0.0296	1.96	0.90	0.038
C2-H18	Σ	1.9858	C3-N5	σ*	0.0844	1.98	0.97	0.040
C3-N4	Σ	1.9831	C3-O8	π*	0.0119	1.30	1.42	0.038
	Σ		N5-C7	σ*	0.0152	3.12	1.14	0.053
C3-N5	Σ	1.9830	C3-O8	π*	0.0119	1.30	1.42	0.038
C3-O8	Σ	1.9948	N4-C6	σ*	0.0152	3.12	1.14	0.053
	Σ		C3-O8	σ*	0.3779	2.20	0.38	0.029
C3-O8	Π	1.9931	C1-N4	σ*	0.0204	1.07	1.40	0.035
	Π		C3-N5	σ*	0.0844	1.46	1.49	0.042
N4-C6	Σ	1.9881	C3-N5	σ*	0.0844	1.44	1.18	0.037
N5-C7	Σ	1.9881	C3-N4	σ*	0.0844	1.44	1.18	0.0.37
C6-H9	Σ	1.9906	C3-N4	σ*	0.0844	2.75	0.96	0.047
C6-H10	Σ	1.9915	C3-N4	σ*	0.0844	0.54	0.95	0.021
C6-H11	Σ	1.9879	C1-N4	σ*	0.0204	4.40	0.86	0.055
C7-H12	Σ	1.9906	C3-N5	σ*	0.0844	2.75	0.96	0.047
C7-H13	Σ	1.9915	C3-N5	σ*	0.0844	0.54	0.95	0.021
C7-H14	Σ	1.9879	C2-N5	σ*	0.0204	4.40	0.86	0.055
N4	LP	1.7444	C1-H15	σ*	0.0296	7.54	0.64	0.066
	LP		C3-O8	σ*	0.3779	50.63	0.29	0.111
N5	LP	1.7444	C2-H17	σ*	0.0296	7.54	0.64	0.066
	LP		C3-O8	σ*	0.3779	50.64	0.29	0.111
O8	LP	1.9781	C3-N5	σ*	0.0844	1.85	1.11	0.041
O8	LP	1.8408	C3-N5	σ*	0.0844	25.08	0.68	0.118

a E(2) means energy of hyper conjugative interaction (stabilization energy).
b Energy difference between donor and acceptor i and j NBO orbitals.
c F(i,j) is the Fock matrix element between i and j NBO orbitals.

The orbital occupancy data and delocalization energy provide valuable information about the electron environment and stabilization. From the NBO analysis, stabilization energy

is maximum for n1 (N6) → π*(C3-O8), n_1 (N5) → π*(C3-O8), and n_1 (O8) → π*(C3-N5) with stabilization energies 50.63, 50.64 and 23.08 kcal/mol respectively. The NBO result is tabulated in Table 4.

Scientists engaged in the molecular electronics field are continuously searching for molecules with substantial nonlinear optical activity. Such compounds find immense applications in electronic display, surveillance equipment, and routine electronic gadgets. Computationally, a molecule's ability to act as an NLO material can be generated from the polarisability and hyperpolarizability data [22-28]. The electric dipole moment, first-order, and second-order polarizabilities are 2.6109 debyes, 23.65561×10^{-24}esu, and 1.51451×10^{-30} esu, respectively. The corresponding list of NLO properties is shown in Table 5.

Table 5. The electric dipole moment (D), average polarizability, first hyperpolarizability, etc., for N-N'-dimethylethylene urea.

μ and α components	**B3LYP/6-311++G****	***β* components**	**B3LYP/6-311++G****
μ_x	-0.0003	β_{xxx}	-0.0101
μ_y	1.6157	β_{xxy}	-64.4969
μ_z	0.000009	β_{xyy}	-0.0019
μ(D)	2.6107	β_{yyy}	148.3545
α_{xx}	92.0035	β_{xxz}	-0.0113
α_{xy}	0.00004	β_{xyz}	-4.3684
α_{yy}	82.7754	β_{yyz}	-0.0081
α_{xz}	1.7840	β_{xzz}	-0.0027
α_{yz}	-0.00008	β_{yzz}	91.4439
α_{zz}	61.5327	β_{zzz}	0.0037
Δα	23.6556×10^{-24}esu		
α_0(esu)	11.6736×10^{-24}	βtotal (esu)	1.5145×10^{-30}

3.5. Noncovalent interactions (NCI), reduced density gradient (RDG), and Laplacian of electron density (LED) for N-N'-dimethylethylene urea.

A noncovalent interaction differs from a covalent bond by not involving electrons' sharing but involving more dispersed variations of electromagnetic interactions between molecules or within a molecule [11,43–46]. The three-dimensional arrangement of large molecules, such as protein and nucleic acids, is important to noncovalent interactions. Additionally, they are also involved in many biological processes where large molecules bind to each other specifically but transiently. These interactions also have a strong impact on drug design, crystallinity and material design, self-assembly, and the design of synthesis of tailor-made organic molecules. The noncovalent interactions for N-N'-dimethylethylene urea are shown in Figure 6. A graph plotted energy (from -0.014 to 0.042 a.u.) against a reduced density gradient (from 0.850 to 1.200). The strong hydrogen bonds having negative energy between the range -0.015 and -0.013 a.u. between nitrogen in imidazole- and hydrogens in N-acetyl-groups, van der Waals force attraction is a weak hydrogen bonds energy between -0.005 and 0.005 a.u. from carbonyl- oxygen to N-acetyl- hydrogens, and steric force is a weak repulsive force of energy between the range 0.005 and 0.042 a.u. for imidazole- ring, and between carbonyl- oxygen, and N-acetyl- groups.

The reduced density gradient is directly proportional to the molecule's electronic density, which means a small reduced density gradient is low electronic density [43,46–49]. Figure 6 shows the reduced density gradient for N-N'-dimethylethylene urea, from the blue to red as the numerical values between 0.000 and 1.000, and the molecule within ± 7.45 $Bohr^3$ range. The red shows the high electronic reduced density between 0.9000 and 1.000 on the

elements between carbonyl-oxygen, and N-acetyl- groups, and all the heavy atoms are nitrogens and carbons in the imidazole- group. The small reduced density gradients shown in color blue are low reduced densities from 0.000 to 0.200 mingle with low reduced density gradients in imidazole-ring shown in Figure 6.

The Laplacian of electron density is the absolute difference from the mean [50,51]. Figure 6 shows the Laplacian of electron density for N-N'-dimethylethylene urea., from blue to red as the numerical values between -8.000 and 15.000, and the molecule within ± 6.56 $Bohr^3$ range. The blue between the ranges -5.700 and -3.400 show the negative Laplacian electron density on carbonyl-oxygen, -0.900 and 0.600 on hydrogens in N-acetyl- groups, and electrophiles can easily attack these sites. The red in the color range between 12.700 and 15.000 shows positive Laplacian electron density on nitrogens and carbons in the molecule, so nucleophiles can easily attack these sites.

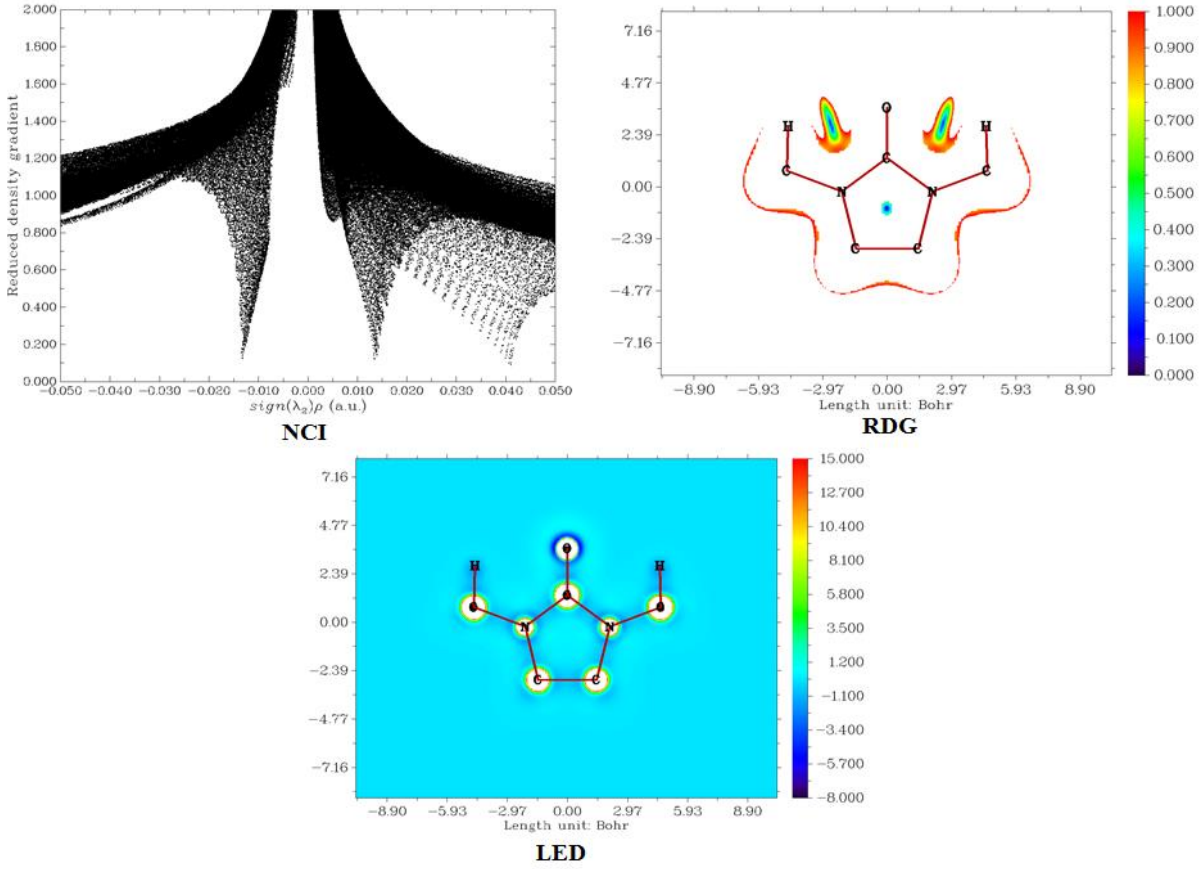

Figure 6. Noncovalent interactions, reduced density gradient, and Laplacian of electron density of N-N'-dimethylethylene urea.

3.6. Molecular electrostatic potentials (MESP) for N-N'-dimethylethylene urea from electronic and molecular charges.

The electrostatic potential V(r) generated around a molecule by its nuclei and electrons treated as static charge distribution is a very useful property for studying and predicting molecular-reactive actions. This is narrowly defined and can be calculated both experimentally and computationally. The capacity has been especially useful for indicating the molecule's positions or regions to which the advancing electrophile is initially drawn. It has also been effectively extended to analyze associations requiring a certain optimal relative orientation of the reactants, such as between the product and its cellular receptor [52–55]. N-

N'dimethylethylenurea molecule's MESP was generated using the data obtained in the previous calculation and is represented in Figure 7.

The blue appears on the oxygen, and nitrogen atoms ring (electrophilic region) in the imidazole- group, which are electron-rich sites, so electrophiles can easily attack these sites. The red color appears on all the protons in the nitrogen atoms and carbon atoms in the imidazole (nucleophilic region) group. These are electrons poor sites, so nucleophiles can easily attack these sites.

The nuclear charge between 12.500 and 15.000 are indicated by blue color, which means repulsion between protons and nuclei in the absence of neutrons as in hydrogen. These sites mostly undergo substitution reactions. The nuclear charge between 45 and 50 is indicated using red, which is negative electrostatic potential with strong attractions between protons and nuclei by core and lone-pair of electrons in heavy atoms like oxygen, nitrogen, and carbon in the molecule, and these sites mostly undergo addition reactions.

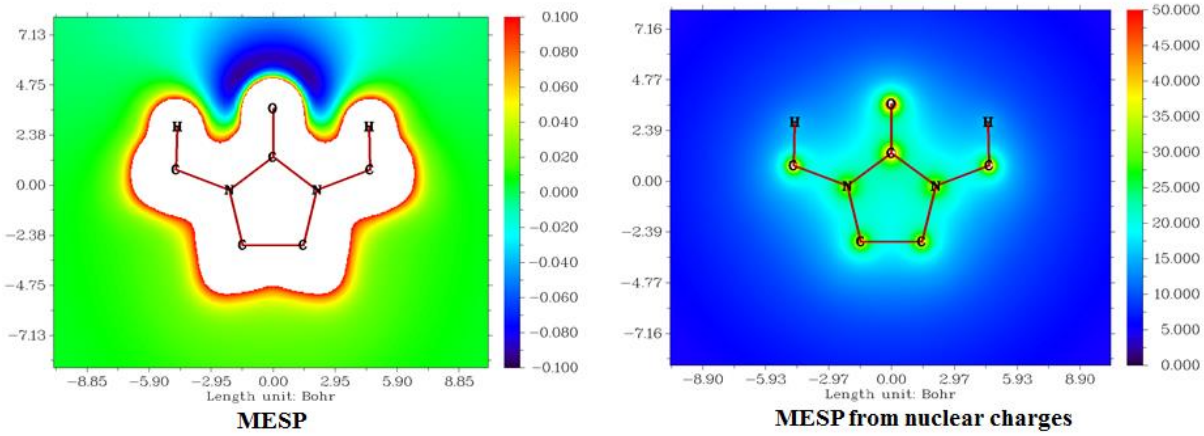

Figure 7. Molecular electrostatic potentials from electronic and nuclear charges of N-N'-dimethylethyleneurea

3.7. Electron localized function (ELF), and localized orbital locator (LOL) for N-N'-dimethylethylene urea.

Electron localized function study explains further the electronic structure for N-N'-dimethylethylene urea. The higher value of the electron localization function is strongly localized, and the low value is a strong delocalization of electrons in this molecule [56–58]. The electron localized function (ELF) for N-N'-dimethylethylene urea is shown in Figure 8, from blue to red as the numerical values between 0.000 and 0.100, and the molecule within ± 8.93 $Bohr^3$ range. The color red between the range 0.850 and 1.000 shows the highest probability of localized electrons occurs on all the hydrogen atoms, and core electrons in heavy atoms are oxygen, nitrogens, and carbons in the molecule. The color blue between the range 0.000 and 0.200 shows the highest probability of delocalized electrons occurs in imidazole-ring, and valance and lone-pairs of electrons in heavy atoms are hydrogen, nitrogens, and carbons in the molecule.

The localized orbital locator (LOL) study explains the localized and delocalized molecular orbitals locations for N-N'-dimethylethylene urea [56–58]. The localized orbital locator (LOL) for N-N'-dimethylethylene urea is shown in Figure 8, from blue to red as the numerical values between 0.000 and 0.800, and the molecule within ± 8.92 $Bohr^3$ range. The blue color denotes weak pi-delocalized orbital, and the red color denotes strong pi-delocalized orbitals in N-N'-dimethylethylene urea; in this molecule, these orbitals appear adjacently, so delocalization of electrons occurs on oxygen, nitrogens, and carbons in the molecule.

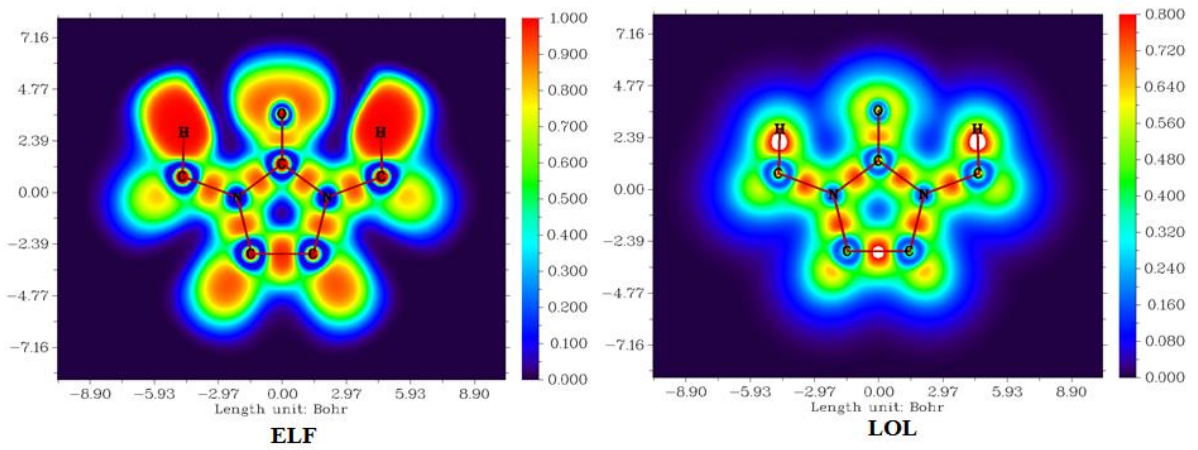

Figure 8. Electron localized function and local orbital locator of N-N'-dimethylethylene urea.

3.8. Average localized ionization energy (ALIE) and local information entropy (LIE) study for N-N'-dimethylethylene urea.

The local I(r) average energy of ionization is the energy needed to remove an electron from point r into the system. The lowest values show the least tightly-held electrons' positions and, therefore, the chosen reaction sites with electrophiles or radicals. Beyond its importance to reactive behavior, I(r) plays a significant role in other fundamental fields, including atomic shell composition, electronegativity, local polarizability, and hardness [59–62]. The pictorial representation of ALIE of N-N'-dimethylethylene urea is given in Figure 9, from blue to red as the numerical values between 0.000 and 2.000, and the molecule within ± 7.34 $Bohr^3$ range. The color bluish-green range between 0.700 and 0.900 indicates moving electrons or delocalization of electrons in N-N'-dimethylethylene urea molecule at the sites are carbonyl oxygen, and acetyl- groups imidazole- group, which produce resonance structures and make the molecule stable. The blue indicates the sigma bond as well as the stable bond between carbons and hydrogens, carbon and nitrogen, and carbon and carbon, and lone-pair of electrons of carbonyl- oxygen, which the sites are from protons to carbons in the whole molecule, and lone pair of electrons having oxygens and nitrogen in purin- and methoxyphenyl- groups.

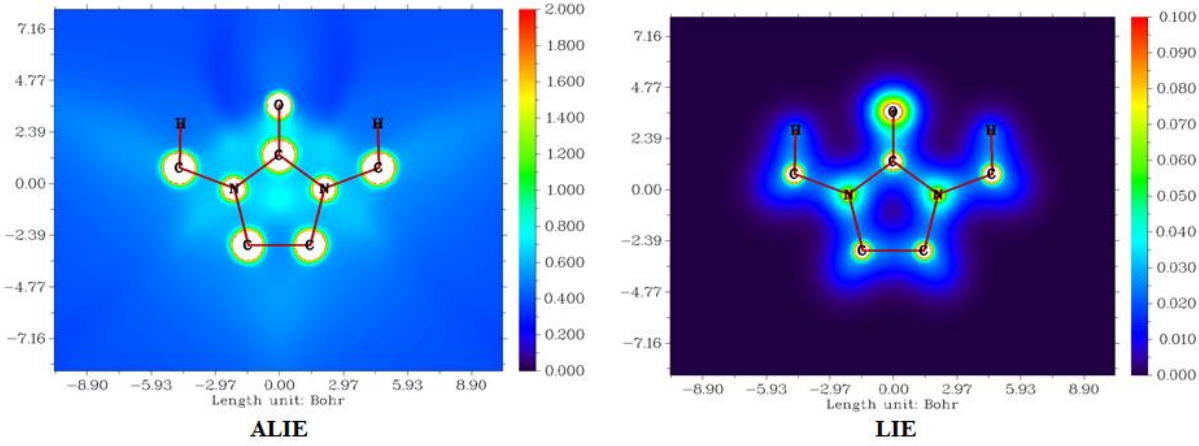

Figure 9. Average localized ionization energy and local information entropy of N-N'-dimethylethylene urea.

The local information entropy (LIE) study explains the stability of the molecule. Entropy is a feature of probability distributions and can take to be a qualification of uncertainty. The high value of local information entropy is directionally proportional to electrons' uncertainty in spatial distribution [37-40]. Figure 9 shows local information entropy for N-N'-

dimethylethylene urea, from the blue to red as the numerical values between 0.000 and 1.000, and the molecule within ± 7.45 $Bohr^3$ range. The color blue between the range 0.000 and 0.020 has low entropy values, which is explain the very low uncertainty of the elements are all the hydrogen in the molecule. The color red between the range 0.085 to 0.100 has high entropy values, which is explain high uncertainty of the heavy elements are oxygen, nitrogens, and carbons in the molecule.

3.9. Inclusion complex with cyclodextrins.

Biological activity prediction and molecular docking studies indicate that our compound can be developed as methylhydantoinase inhibitor for clinical applications. Drug delivery is a critical issue to be addressed when it is developed as a drug. Here, we attempt to make an active complex of the drug NND with γ-cyclodextrin (CD). The drug is placed inside the CD and optimized to a minimum. As the complex formation involves bulky molecules, there is a possibility of dispersion interactions; hence we have incorporated the dispersion corrections to the B3LYP functional using Grimme's dispersion correction using 6-31G (d) basis set [63–67]. The data presented in Table 6 indicates that dispersion is a significant factor to be considered while modeling molecular inclusion systems. The dispersion energy for the complex is 9.09 kcal/mol, which is an appreciable amount of energy that confirms that appreciable dispersion interaction exists in the complex, as expected. The optimized geometry of the complex is provided in Figure 10. The distance between the carbonyl oxygen of NND and the nearest hydrogen atom of the CD in the complex is 2.5863A. Furthermore, to investigate the driving forces of NND in γ-CD , we have calculated the complexation energy, HOMO, and LUMO energies, chemical reactivity defined as per the following equation.

$$\Delta E_{complexation} = E^{opt}complex - [E(\gamma\text{-CD})^{opt}_{free} + E(NND)]^{opt}_{free} \quad (1)$$

From the data, the complexation energy is found to be -56.4949791 kcal/mol, which is appreciable energy.

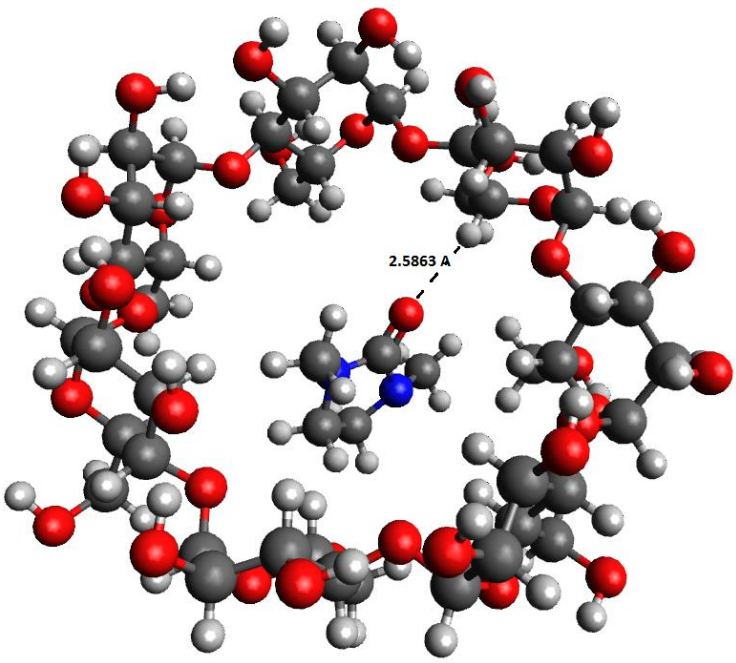

Figure 10. NND- CD complex optimized at B3LYP/6-31G(d) with Griumme's dispersion correction.

Table 6. Molecular recognition energy between NND and CD with and without dispersion correction.

System	B3LYP/6-31G(d)	B3LYP/6-31G(d) with Grimme's dispersion correction
NND	-381.1799371	-381.1925119
γ-cyclodextrin	-4275.18	-4275.42
NND-CD Complex	-4656.435218	-4656.702187
Energy of Inclusion	-0.07528082	-0.08967457
(kcal/mol)	-47.4269166	-56.4949791

3.10. Molecular docking studies of NND.

The biological activity of NND was shown in Table 7 from the PASS online site. N-methylhydantoinase (ATP-hydrolysing) inhibitor has the topmost probability of being active with a very low probability of inactive values corresponding PDB ID: 3I73 [68] downloaded and prepared to dock undock with NND molecule by both online servers SwissDock and PatchDock. The result from the SwissDock server shown in Table 8 explains full fitness energy -2675.96 kcal/mol, total ΔG energy -5.89 kcal/mol, as well as inter full fitness, intra full fitness, full solvent fitness, full surface fitness, ΔG of complex solvent polar, complex solvent non-polar, protein solvent polar, protein solvent non-polar, ligand solvent polar, ligand solvent non-polar, van der Waals force and electrical fore energies for interactions between NND and protein with the unit of kcal/mol.

Table 7. Biological activity prediction of NND using PASS.

Pa	Pi	Activity
0.87	0.002	N-methylhydantoinase (ATP-hydrolysing) inhibitor
0.87	0.004	Nicotinic alpha6beta3beta4alpha5 receptor antagonist
0.865	0.004	Nicotinic alpha2beta2 receptor antagonist
0.844	0.015	Testosterone 17beta-dehydrogenase (NADP+) inhibitor
0.845	0.018	Phobic disorders treatment
0.815	0.004	Phospholipid-translocating ATPase inhibitor
0.807	0.012	Glycosylphosphatidylinositol phospholipase D inhibitor
0.791	0.003	Kidney function stimulant
0.797	0.013	NADPH peroxidase inhibitor

Table 8. Thermodynamic data from molecular docking**.**

Full Fitness	-2675.964 kcal/mol
Inter Full Fitness	-20.2328 kcal/mol
Intra Full Fitness	-28.1168 kcal/mol
Solvent Full Fitness	-2984.41 kcal/mol
Surface Full Fitness	356.796 kcal/mol
Extra Full Fitness	0 kcal/mol
ΔG complex solvent polar	-2984.41 kcal/mol
ΔG complex solvent non-polar	356.796 kcal/mol
ΔG protein solvent polar	-2985.62 kcal/mol
ΔG protein solvent non-polar	357.709 kcal/mol
ΔG ligand solvent polar	-6.44042 kcal/mol
ΔG ligand solvent non-polar	3.93924 kcal/mol
ΔG van der Waals fore	-20.2328 kcal/mol
ΔG electrical force	0 kcal/mol
Total ΔG	-5.894829 kcal/mol

The result from PatchDock having the score value 2656, area 287.20 $(Å)^2$ and minimum atomic contact energy -79.28 kcal/mol between NND and referred protein. The BioDiscovery

Studio 2017 software is used for interpreting interactions between NND and protein [14,15,69–75].

3.10.1. Interactions between NND and protein.

Figure 11 shows skeletal structure interactions between NND and protein residues with the types and bond distances, and Figure 12 interactions between NND and protein residues with the label. Table 9 explains all types of interacting protein residues with NND having hydrophobicity value, average isotropic displacement, secondary structure, residue solvent accessibility, sidechain solvent accessibility, percent solvent accessibility, and percent sidechain solvent accessibility. Table 10 explains the favorable non-bond interaction category, type, chemistry, and bond distances between NND and protein residues. There are also unsatisfied bond oxygen atoms in the NND molecule.

Figure S1 and Table 9 explain hydrophobic interactions between NND and protein residues. Figure S2 and Table 9 explain hydrophilic and acidic group interactions between NND and protein residues. There is no basic group interaction between NND and protein. Figure S3 and Table 9 explain neutral group interactions between NND and protein residues [76–84].

Table 9. Interactions between NND and protein residues.

Name	Label	Hydrophobicity	Average Isotropic Displacement (Å)^2	Secondary structure	Residue Solvent Accessibility(Å)^2	Sidechain Solvent Accessibility(Å)^2	Percent Solvent Accessibility(Å)^2	Percent sidechain Solvent Accessibility (Å)^2
Isoleucine	A:Ile84	4.5	65.899	Sheet	47.513	40.757	29.737	35.92
Leucine	A:Leu92	3.8	94.684	Sheet	114.885	97.113	75.734	97.722
Glutamic Acid	A:Glu93	-3.5 (pKa 4.3)	99.926	Coil	140.977	110.988	79.933	89.926
Methionine	A:Met268	1.9	113.007	Turn	86.602	69.606	47.593	53.951
Valine	A:Val271	4.2	110.919	Turn	49.28	48.808	35.043	55.508
Leucine	A:Leu272	3.8	109.171	Turn	91.698	86.044	60.449	86.582
Alanine	A:Ala295	1.8	67.386	Coil	23.13	21.133	23.103	45.902
Threonine	A:Thr297	-0.7	75.843	Coil	27.507	17.611	20.745	20.411
Methionine	A:Met300	1.9	79.882	Coil	100.457	31.465	55.207	24.388

Table 10. Favorable non-bond between NND and protein residues.

Distance (Å)	Category	Type	From	From Chemistry	To	To Chemistry
2.76967	Hydrogen Bond	Carbon Hydrogen Bond	:UNK0:H	H-Donor	A:MET268:O	H-Acceptor
2.62026	Hydrogen Bond	Carbon Hydrogen Bond	:UNK0:H	H-Donor	A:GLU93:OE2	H-Acceptor
4.37675	Hydrophobic	Alkyl	A:ALA295	Alkyl	:UNK0	Alkyl
4.46229	Hydrophobic	Alkyl	A:ALA295	Alkyl	:UNK0:C	Alkyl
3.99483	Hydrophobic	Alkyl	:UNK0:C	Alkyl	A:LEU92	Alkyl
4.41282	Hydrophobic	Alkyl	:UNK0:C	Alkyl	A:VAL271	Alkyl
2.76967	Hydrogen Bond	Carbon Hydrogen Bond	:UNK0:H	H-Donor	A: MET268: O	H-Acceptor
2.62026	Hydrogen Bond	Carbon Hydrogen Bond	:UNK0:H	H-Donor	A:GLU93:OE2	H-Acceptor
4.37675	Hydrophobic	Alkyl	A:ALA295	Alkyl	:UNK0	Alkyl
4.46229	Hydrophobic	Alkyl	A:ALA295	Alkyl	:UNK0:C	Alkyl

Distance (Å)	Category	Type	From	From Chemistry	To	To Chemistry
3.99483	Hydrophobic	Alkyl	:UNK0:C	Alkyl	A:LEU92	Alkyl
4.41282	Hydrophobic	Alkyl	:UNK0:C	Alkyl	A:VAL271	Alkyl

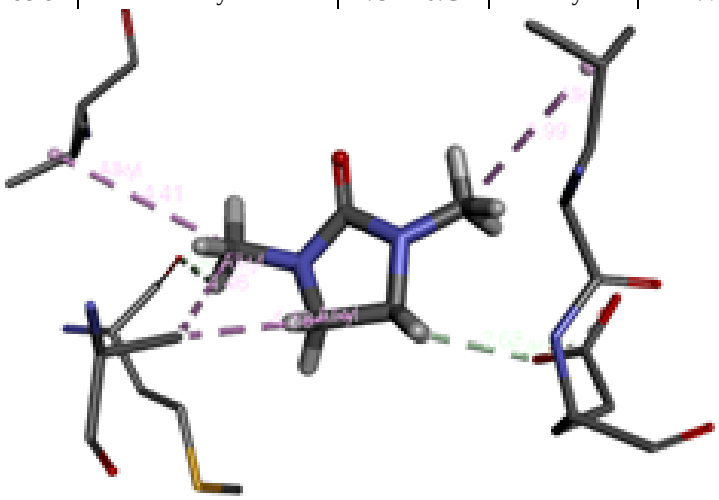

Figure 11. Skeletal structural interactions between N-N'-dimethylethylene urea and protein.

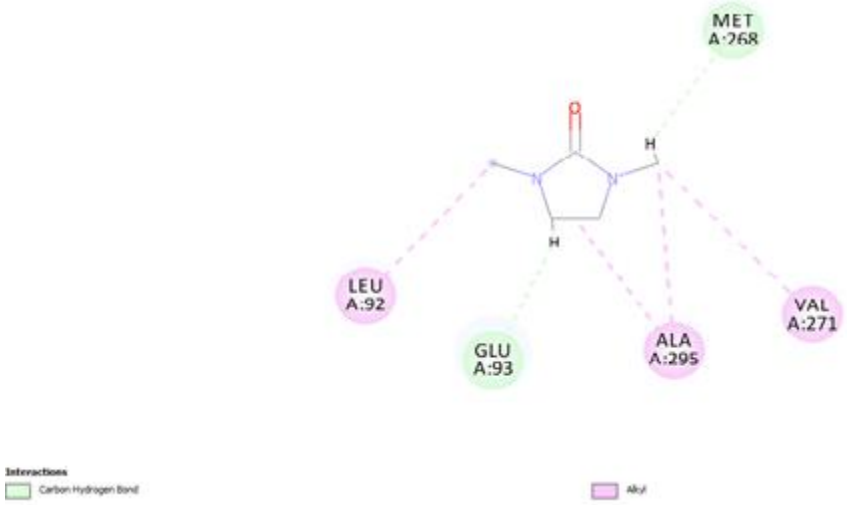

Figure 12. Interactions between N-N'-dimethylethylene urea and protein residues.

4. Conclusions

N-N'-dimethylethylene urea was characterized by IR, Raman, and UV-Vis spectra. The simulated and experimental spectra showed a close correlation. Vibrational modes are assigned based on the PED matrix. Scaled wave numbers are in good agreement with experimental wave numbers. The compound is stabilized by various intramolecular interactions and shows excellent hyperpolarizabilities indicating that it could be a potential NLO material. All electron descriptor analyses are in conformation with the reactivity details. Docking studies indicate that the molecule can be used as a methylhydantoinase (ATP-hydrolysing) inhibitor. The inclusion energy data shows that the molecule can be placed inside the cavity of a cyclodextrin molecule.

Funding

A. Irfan extends his appreciation to the Deanship of Scientific Research at King Khalid University Saudi Arabia through General Research Project under grant number (GRP/17/42).

Acknowledgments

A. Irfan extends his appreciation to the Deanship of Scientific Research at King Khalid University Saudi Arabia through General Research Project under grant number (GRP/17/42).

Conflicts of Interest

The authors declare no conflicts of interest.

References

1. Finar, I. L. *Organic Chemistry*, 6th ed.; Great Britain by Richard Clay and Company, Ltd., Bungay, Suffolk, 1961.
2. Bruno, O.; Brullo, C.; Bondavalli, F.; Schenone, S.; Ranise, A.; Arduino, N.; Bertolotto, M. B.; Montecucco, F.; Ottonello, L.; Dallegri, F.; Tognolini, M.; Ballabeni, V.; Bertoni, S.; Barocelli, E.; Farmaceutiche, S.; Uni, V.; Xv, V. B.; Interna, M.; Uni, V. Synthesis and Biological Evaluation of N -Pyrazolyl- N ′ -Alkyl / Benzyl / Phenylureas : A New Class of Potent Inhibitors of Interleukin 8-Induced Neutrophil Chemotaxis. *J. Med. Chem.* **2007**, *50*, 3618–3626. https://doi.org/10.1021/jm0704402.
3. Jose N. Domınguez; Caritza Leon; Juan Rodrigues; Neira Gamboa de Domınguez; Jiri Gut, P. J. R. Synthesis and Evaluation of New Antimalarial Phenylurenyl Chalcone Derivatives. *J. Med. Chem.* **2005**, *48*, 3654–3658. https://doi.org/10.1021/jm058208o.
4. Sahlberg, C.; Norren, R.; Engelhardt, P.; Hrgberg, M.; Kangasmets, J.; Vrang, L.; Zhang, H.; Ab, M.; Huddinge, S. Synthesis and Anti-HIV Activities of Urea-PETT Analogs Belonging to a New Class of Potent Non- Nucleoside HIV-1 Reverse Transcriptase Inhibitors. *Bioorg. Med. Chem. Lett.* **1998**, *8*, 1511–1516. https://doi.org/10.1016/S0960-894X(98)00249-2.
5. Mustafa, S.; Perveen, S.; Khan, A. Synthesis, Enzyme Inhibition and Anticancer Investigations of Unsymmetrical 1,3-disubstituted Ureas. *J. Serbian Chem. Soc.* **2014**, *79*, 1–10. https://doi.org/10.2298/JSC121212076M.
6. Kim, I.; Morisseau, C.; Watanabe, T.; Hammock, B. D. Design , Synthesis , and Biological Activity of 1 , 3-Disubstituted Ureas as Potent Inhibitors of the Soluble Epoxide Hydrolase of Increased Water Solubility. *J. Med. Chem.* **2004**, *47*, 2110–2122. https://doi.org/10.1021/jm030514j.
7. Shaaban, I. A. Conformational Analysis, Infrared/Raman Spectral Assignment, and Electronic Structural Studies of 1,3-Dimethyl-2-Imidazolidinone Using Quantum Chemical Calculations. *J. Mol. Struct.* **2019**, *1175*, 708–720. https://doi.org/10.1016/j.molstruc.2018.08.015.
8. Alharthi, F. A.; Al-Zaqri, N.; Alsalme, A.; Al-Taleb, A.; Pooventhiran, T.; Thomas, R.; Rao, D. J. Excited-State Electronic Properties, Structural Studies, Noncovalent Interactions, and Inhibition of the Novel Severe Acute Respiratory Syndrome Coronavirus 2 Proteins in Ripretinib by First-Principle Simulations. *J. Mol. Liq.* **2021**, *324*, 115134. https://doi.org/10.1016/j.molliq.2020.115134.
9. Ullah, Z.; Thomas, R. Markovnikov versus Anti-Markovnikov Addition and C–H Activation: Pd–Cu Synergistic Catalysis. *Appl. Organomet. Chem.* **2021**, *35*, e6077. https://doi.org/10.1002/aoc.6077.
10. Alsalme, A.; Pooventhiran, T.; Al-Zaqri, N.; Rao, D. J.; Thomas, R. Structural, Physico-Chemical Landscapes, Ground State and Excited State Properties in Different Solvent Atmosphere of Avapritinib and Its Ultrasensitive Detection Using SERS/GERS on Self-Assembly Formation with Graphene Quantum Dots. *J. Mol. Liq.* **2021**, *322*, 114555. https://doi.org/10.1016/j.molliq.2020.114555.
11. Al-Zaqri, N.; Pooventhiran, T.; Rao, D. J.; Alsalme, A.; Warad, I.; Thomas, R. Structure, Conformational Dynamics, Quantum Mechanical Studies and Potential Biological Activity Analysis of Multiple Sclerosis Medicine Ozanimod. *J. Mol. Struct.* **2021**, *1227*, 129685. https://doi.org/10.1016/j.molstruc.2020.129685.
12. Al-Otaibi, J. S.; Mary, Y. S.; Armaković, S.; Thomas, R. Hybrid and Bioactive Cocrystals of Pyrazinamide with Hydroxybenzoic Acids: Detailed Study of Structure, Spectroscopic Characteristics, Other Potential Applications and Noncovalent Interactions Using SAPT. *J. Mol. Struct.* **2020**, *1202*, 127316. https://doi.org/10.1016/j.molstruc.2019.127316.
13. Al-Otaibi, J. S.; Almuqrin, A. H.; Sheena Mary, Y.; Mary, Y. S.; Thomas, R. Modeling the Conformational Preference, Spectral Analysis and Other Quantum Mechanical Studies on Three Bioactive Aminobenzoate Derivatives and Their SERS Active Graphene Complexes. *Polycycl. Aromat. Compd.* **2020**, 1–11. https://doi.org/10.1080/10406638.2020.1827270.
14. Haruna, K.; Kumar, V. S.; Armaković, S. J.; Armaković, S.; Mary, Y. S.; Thomas, R.; Popoola, S. A.;

Almohammedi, A. R.; Roxy, M. S.; Al-Saadi, A. A. Spectral Characterization, Thermochemical Studies, Periodic SAPT Calculations and Detailed Quantum Mechanical Profiling Various Physico-Chemical Properties of 3, 4-Dichlorodiuron. *Spectrochim. Acta Part A Mol. Biomol. Spectrosc.* **2020**, *228*, 117580. https://doi.org/10.1016/j.saa.2019.117580.

15. Al-Otaibi, J. S.; Almuqrin, A. H.; Mary, Y. S.; Mary, Y. S.; Thomas, R. Cocrystals of Hydrochlorothiazide with Picolinamide, Tetramethylpyrazine and Piperazine: Quantum Mechanical Studies, Docking and Modelling of the Photovoltaic Efficiency for DSSC. *J. Mol. Model.* **2020**, *26*, 256. https://doi.org/10.1007/s00894-020-04528-9.
16. Kanchana, U. S.; Diana, E. J.; Mathew, T. V; Anilkumar, G. Cyclodextrin Based Palladium Catalysts for Suzuki Reaction: An Overview. *Carbohydr. Res.* **2020**, *489*, 107954. https://doi.org/10.1016/j.carres.2020.107954.
17. Diana, E. J.; Kanchana, U. S.; Mathew, T. V; Anilkumar, G. Recent Developments in the Metal Catalysed Cross-Coupling Reactions for the Synthesis of the Enone System of Chalcones. *Appl. Organomet. Chem.* **2020**, *34*, e5987. https://doi.org/10.1002/aoc.5987.
18. Jose, D. E.; Kanchana, U. S.; Mathew, T. V; Anilkumar, G. Recent Studies in Suzuki-Miyaura Cross-Coupling Reactions with the Aid of Phase Transfer Catalysts. *J. Organomet. Chem.* **2020**, *927*, 121538. https://doi.org/10.1016/j.jorganchem.2020.121538.
19. Kanchana, U. S.; Diana, E. J.; Mathew, T. V; Anilkumar, G. Palladium-Catalyzed Cross-Coupling Reactions of Coumarin Derivatives: An Overview. *Appl. Organomet. Chem.* **2020**, *34* (12), e5983. https://doi.org/10.1002/aoc.5983.
20. Jose, D. E.; Kanchana, U. S.; Mathew, T. V.; Anilkumar, G. Recent Developments and Perspectives in the C-Se Cross Coupling Reactions. *Current Organic Chemistry*. **2020**, *24*, 1230–1262. http://dx.doi.org/10.2174/1385272824999200528130131.
21. Kanchana, U. S.; Mathew, T. V; Anilkumar, G. Recent Advances and Prospects in the Nickel- Catalyzed Cyanation. *J. Organomet. Chem.* **2020**, *920*, 121337. https://doi.org/10.1016/j.jorganchem.2020.121337.
22. M. J. Frisch, G. W. Trucks, H. B. Schlegel, G. E. Scuseria, M. A. Robb, J. R. Cheeseman, G. Scalmani, V. Barone, G. A. Petersson, H. Nakatsuji, X. Li, M. Caricato, A. Marenich, J. Bloino, B. G. Janesko, R. Gomperts, B. Mennucci, H. P. Hratchian, J. V. Ort, D. J. F. Gaussian09W Revision D.01. Gaussian, Inc., Wallingford CT, 2016. **2009**.
23. Becke, A. D. Density-Functional Exchange-Energy Approximation with Correct Asymptotic Behavior. *Phys. Rev. A* **1988**, *38*, 3098. https://doi.org/10.1103/PhysRevA.38.3098.
24. Becke, A. D. A New Mixing of Hartree-Fock and Local Density-Functional Theories. *J. Chem. Phys.* **1993**, *98*, 1372–1377. https://doi.org/10.1063/1.464304.
25. Becke, A. D.; Johnson, E. R. A Density-Functional Model of the Dispersion Interaction. *J. Chem. Phys.* **2005**, *123*, 154101. https://doi.org/10.1063/1.2065267.
26. Becke, A. D. Perspective: Fifty Years of Density-Functional Theory in Chemical Physics. *J. Chem. Phys.* **2014**, *140*, 18A301. https://doi.org/10.1063/1.4869598.
27. Becke, A. D. Density-functional Thermochemistry. III. The Role of Exact Exchange. *J. Chem. Phys.* **1993**, *98*, 5648–5652. https://doi.org/10.1063/1.464913.
28. Krishnan, R.; Binkley, J. S.; Seeger, R.; Pople, J. A. Self-consistent Molecular Orbital Methods. XX. A Basis Set for Correlated Wave Functions. *J. Chem. Phys.* **1980**, *72*, 650–654. https://doi.org/10.1063/1.438955.
29. Longuet-Higgins, H. C.; Pople, J. A. Electronic Spectral Shifts of Non-polar Molecules in Non-polar Solvents. *J. Chem. Phys.* **1957**, *27*, 192–194. https://doi.org/10.1063/1.1743666.
30. Frisch, M. J.; Pople, J. A.; Binkley, J. S. Self-consistent Molecular Orbital Methods 25. Supplementary Functions for Gaussian Basis Sets. *J. Chem. Phys.* **1984**, *80*, 3265–3269. https://doi.org/10.1063/1.447079.
31. Rassolov, V. A.; Ratner, M. A.; Pople, J. A.; Redfern, P. C.; Curtiss, L. A. 6-31G* Basis Set for Third-Row Atoms. *J. Comput. Chem.* **2001**, *22*, 976–984. https://doi.org/10.1002/jcc.1058.
32. Friesner, R. A. Ab Initio Quantum Chemistry: Methodology and Applications. *Proc. Natl. Acad. Sci. U. S. A.* **2005**, *102*, 6648–6653. https://doi.org/10.1073/pnas.0408036102.
33. ED Glendening, AE Reed, JE Carpenter, F. W. NBO 3.1. Theoretical Chemistry Institute, University of Wisconsin, Madison 2003.
34. O'boyleO'boyle, N. M.; Tenderholt, A. L.; Langner, K. M. CCLIB: A Library for Package-Independent Computational Chemistry Algorithms. *J. Comput. Chem.* **2008**, *29*, 839–845. https://doi.org/10.1002/jcc.20823.
35. Lu, T.; Chen, F. Multiwfn: A Multifunctional Wavefunction Analyzer. *J. Comput. Chem.* **2012**, *33*, 580–

592. https://doi.org/10.1002/jcc.22885.
36. Lagunin, A.; Stepanchikova, A.; Filimonov, D.; Poroikov, V. PASS: Prediction of Activity Spectra for Biologically Active Substances. *Bioinformatics* **2000**, *16*, 747–748. https://doi.org/10.1093/bioinformatics/16.8.747.
37. Hajji, M.; Mtiraoui, H.; Amiri, N.; Msaddek, M.; Guerfel, T. Crystallographic and First-Principles Density Functional Theory Study on the Structure, Noncovalent Interactions, and Chemical Reactivity of 1,5-Benzodiazepin-2-Ones Derivatives. *Int. J. Quantum Chem.* **2019**, *119* , 1–13. https://doi.org/10.1002/qua.26000.
38. Schneidman-Duhovny, D.; Inbar, Y.; Nussinov, R.; Wolfson, H. J. PatchDock and SymmDock: Servers for Rigid and Symmetric Docking. *Nucleic Acids Res.* **2005**, *33*, W363–W367. https://doi.org/10.1093/nar/gki481.
39. Mashiach, E.; Schneidman-Duhovny, D.; Peri, A.; Shavit, Y.; Nussinov, R.; Wolfson, H. J. An Integrated Suite of Fast Docking Algorithms. *Proteins Struct. Funct. Bioinforma.* **2010**, *78*, 3197–3204. https://doi.org/10.1002/prot.22790.
40. Discovery Studio BIOVA. *Discovery Studio Client v17, San Diego, Dassault Systems*. Dassault Systems: SanDeigio 2017.
41. Reed, A. E.; Curtiss, L. A.; Weinhold, F. Intermolecular Interactions from a Natural Bond Orbital, Donor-Acceptor Viewpoint. *Chem. Rev.* **1988**, *88*, 899–926. https://doi.org/10.1021/cr00088a005.
42. Weinhold, F. Natural Bond Orbital Analysis: A Critical Overview of Relationships to Alternative Bonding Perspectives. *J. Comput. Chem.* **2012**, *33*, 2363–2379. https://doi.org/10.1002/jcc.23060.
43. Boto, R. A.; Piquemal, J. P.; Contreras-García, J. Revealing Strong Interactions with the Reduced Density Gradient: A Benchmark for Covalent, Ionic and Charge-Shift Bonds. *Theor. Chem. Acc.* **2017**, *136*, 1–9. https://doi.org/10.1007/s00214-017-2169-9.
44. Karshikoff, A. *Non-Covalent Interactions in Proteins*; World Scientific Publishing Co., 2006. https://doi.org/10.1142/p477.
45. Pooventhiran, T.; Bhattacharyya, U.; Rao, D. J.; Chandramohan, V.; Karunakar, P.; Irfan, A.; Mary, Y. S.; Thomas, R. Detailed Spectra, Electronic Properties, Qualitative Non-Covalent Interaction Analysis, Solvatochromism, Docking and Molecular Dynamics Simulations in Different Solvent Atmosphere of Cenobamate. *Struct. Chem.* **2020**, *31*, 247502485. https://doi.org/10.1007/s11224-020-01607-8.
46. Alsalme, A.; Pooventhiran, T.; Al-Zaqri, N.; Rao, D. J.; Thomas, R. Structural, Physico-Chemical Landscapes, Ground State and Excited State Properties in Different Solvent Atmosphere of Avapritinib and Its Ultrasensitive Detection Using SERS/GERS on Self-Assembly Formation with Graphene Quantum Dots. *J. Mol. Liq.* **2020**, *322*, 114555. https://doi.org/10.1016/j.molliq.2020.114555.
47. Zupan, A.; Perdew, J. P.; Burke, K.; Causà, M. Density-Gradient Analysis for Density Functional Theory: Application to Atoms. *Int. J. Quantum Chem.* **1998**, *61*, 835–845. https://doi.org/10.1002/(SICI)1097-461X(1997)61:5<835::AID-QUA9>3.0.CO;2-X.
48. Del Campo, J. M.; Gázquez, J. L.; Alvarez-Mendez, R. J.; Vela, A. The Reduced Density Gradient in Atoms. *Int. J. Quantum Chem.* **2012**, *112*, 3594–3598. https://doi.org/10.1002/qua.24241.
49. Albrecht, L.; Chowdhury, S.; Boyd, R. J. Hydrogen Bond Cooperativity in Water Hexamers: Atomic Energy Perspective of Local Stabilities. *J. Phys. Chem. A* **2013**, *117*, 10790–10799. https://doi.org/10.1021/jp407371c.
50. Jacobsen, H. Localized-Orbital Locator (LOL) Profiles of Chemical Bonding. *Can. J. Chem.* **2008**, *86*, 695–702. https://doi.org/10.1139/v08-052.
51. Rizwana, F.; Prasana; Christian, J.; Muthu, S.; Abraham, C. S. Molecular Docking Studies, Charge Transfer Excitation and Wave Function Analyses (ESP, ELF, LOL) on Valacyclovir: A Potential Antiviral Drug. *Comput. Biol. Chem.* **2019**, *78*, 9–17. https://doi.org/10.1016/j.compbiolchem.2018.11.014.
52. Breneman, C. M.; Martinov, M. 3 - The Use of Electrostatic Potential Fields in QSAR and QSPR. In *Molecular Electrostatic Potentials*; Murray, J. S., Sen, K. B. T.-T. and C. C., Eds.; Elsevier, **1996**; Vol. 3, pp 143–179. https://doi.org/10.1016/S1380-7323(96)80043-4.
53. Politzer, P.; Laurence, P. R.; Jayasuriya, K. Molecular Electrostatic Potentials: An Effective Tool for the Elucidation of Biochemical Phenomena. *Environ. Health Perspect.* **1985**, *61*, 191–202. https://doi.org/10.1289/ehp.8561191.
54. Politzer, P.; Murray, J. S. Electrostatic Potentials at the Nuclei of Atoms and Molecules. *Theor. Chem. Acc.* **2021**, *140*, 7. https://doi.org/10.1007/s00214-020-02701-0.
55. Politzer, P.; Murray, J. S. Molecular Electrostatic Potentials and Chemical Reactivity. In *Reviews in*

Computational Chemistry. **1991**, 273–312. https://doi.org/10.1002/9780470125793.ch7.
56. Fuster, F.; Sevin, A.; Silvi, B. Topological Analysis of the Electron Localization Function (ELF) Applied to the Electrophilic Aromatic Substitution. *J. Phys. Chem. A* **2000**, *104*, 852–858. https://doi.org/10.1021/jp992783k.
57. Koumpouras, K.; Larsson, J. A. Distinguishing between Chemical Bonding and Physical Binding Using Electron Localization Function (ELF). *J. Phys. Condens. Matter* **2020**, *32*, 315502. https://doi.org/10.1088/1361-648x/ab7fd8.
58. Gibbs, G. V; Cox, D. F.; Boisen Jr., M. B.; Downs, R. T.; Ross, N. L. The Electron Localization Function: A Tool for Locating Favorable Proton Docking Sites in the Silica Polymorphs. *Phys. Chem. Miner.* **2003**, *30*, 305–316. https://doi.org/10.1007/s00269-003-0318-2.
59. Politzer, P.; Murray, J. S.; Bulat, F. A. Average Local Ionization Energy: A Review. *J. Mol. Model.* **2010**, *16*, 1731–1742. https://doi.org/10.1007/s00894-010-0709-5.
60. Politzer, P.; Abu-Awwad, F.; Murray, J. S. Comparison of Density Functional and Hartree–Fock Average Local Ionization Energies on Molecular Surfaces. *Int. J. Quantum Chem.* **1998**, *69*, 607–613. https://doi.org/10.1002/(SICI)1097-461X(1998)69:4<607::AID-QUA18>3.0.CO;2-W.
61. Hossain, M.; Thomas, R.; Mary, Y. S.; K.S.Resmi; Armaković, S.; Armaković, S. J.; Nanda, A. K.; Vijayakumar, G.; Alsenoy, C. Van. Understanding Reactivity of Two Newly Synthetized Imidazole Derivatives by Spectroscopic Characterization and Computational Study. *J. Mol. Struct.* **2018**, *1158*, 176–196. https://doi.org/10.1016/j.molstruc.2018.01.029.
62. Armaković, S.; Armaković, S. J.; Vraneš, M.; Tot, A.; Gadžurić, S. Determination of Reactive Properties of 1-Butyl-3-Methylimidazolium Taurate Ionic Liquid Employing DFT Calculations. *J. Mol. Liq.* **2016**, *222*, 796–803. https://doi.org/10.1016/J.MOLLIQ.2016.07.094.
63. Goerigk, L.; Grimme, S. Efficient and Accurate Double-Hybrid-Meta-GGA Density Functionals- Evaluation with the Extended GMTKN30 Database for General Main Group Thermochemistry, Kinetics, and Noncovalent Interactions. *J. Chem. Theory Comput.* **2011**, *7*, 291–309. https://doi.org/10.1021/ct100466k.
64. Grimme, S.; Hujo, W.; Kirchner, B. Performance of Dispersion-Corrected Density Functional Theory for the Interactions in Ionic Liquids. *Phys. Chem. Chem. Phys.* **2012**, *14*, 4875–4883. https://doi.org/10.1039/C2CP24096C.
65. Grimme, S. Density Functional Theory with London Dispersion Corrections. *Wiley Interdiscip. Rev. Comput. Mol. Sci.* **2011**, *1*, 211–228. https://doi.org/10.1002/wcms.30.
66. Grimme, S.; Ehrlich, S.; Goerigk, L. Effect of the Damping Function in Dispersion Corrected Density Functional Theory. *J. Comput. Chem.* **2011**, *32*, 1456–1465. https://doi.org/10.1002/jcc.21759.
67. Grimme, S. Semiempirical Hybrid Density Functional with Perturbative Second-Order Correlation. *J. Chem. Phys.* **2006**, *124*, 034108. https://doi.org/10.1063/1.2148954.
68. Kumar, A.; Manimekalai, M. S. S.; Balakrishna, A. M.; Jeyakanthan, J.; Grüber, G. Nucleotide Binding States of Subunit A of the A-ATP Synthase and the Implication of P-Loop Switch in Evolution. *J. Mol. Biol.* **2010**, *396*, 301–320. https://doi.org/10.1016/j.jmb.2009.11.046.
69. Al-Zaqri, N.; Pooventhiran, T.; Alsalme, A.; Rao, D. J.; Rao, S. S.; Sankar, A.; Thomas, R. First-Principle Studies of Istradefylline with Emphasis on the Stability, Reactivity, Interactions and Wavefunction-Dependent Properties. *Polycycl. Aromat. Compd.* **2020**, 1–15. https://doi.org/10.1080/10406638.2020.1857273
70. Almuqrin, A. H.; Al-Otaibi, J. S.; Mary, Y. S.; Thomas, R.; Kaya, S.; Işın, D. Ö. Spectral Analysis and Detailed Quantum Mechanical Investigation of Some Acetanilide Analogues and Their Self-Assemblies with Graphene and Fullerene. *J. Mol. Model.* **2020**, *26*, 254. https://doi.org/10.1007/s00894-020-04485-3.
71. Srikanth, K. E.; Veeraiah, A.; Pooventhiran, T.; Thomas, R.; Solomon, K. A.; Raju, C. J. S.; Latha, J. N. L. Detailed Molecular Structure (XRD), Conformational Search, Spectroscopic Characterization (IR, Raman, UV, Fluorescence), Quantum Mechanical Properties and Bioactivity Prediction of a Pyrrole Analogue. *Heliyon* **2020**, *6*, e04106. https://doi.org/10.1016/j.heliyon.2020.e04106
72. Al-Otaibi, J. S.; Almuqrin, A. H.; Mary, Y. S.; Thomas, R. Modeling the Conformational Preference, Spectroscopic Properties, UV Light Harvesting Efficiency, Biological Receptor Inhibitory Ability and Other Physico-Chemical Properties of Five Imidazole Derivatives Using Quantum Mechanical and Molecular Mechanics T. *J. Mol. Liq.* **2020**, *310*, 112871. https://doi.org/10.1016/j.molliq.2020.112871
73. John, A. M.; Jose, J.; Thomas, R.; Thomas, K. J.; Balakrishnan, S. P. Spectroscopic and TDDFT Investigation of Highly Selective Fluoride Sensors by Substituted Acyl Hydrazones. *Spectrochim. Acta Part A Mol. Biomol. Spectrosc.* **2020**, *236*, 118329. https://doi.org/10.1016/j.saa.2020.118329.

74. Priya, Y. S.; Rao, K. R.; Chalapathi, P. V.; Veeraiah, A.; Srikanth, K. E.; Mary, Y. S.; Thomas, R. Intricate Spectroscopic Profiling, Light Harvesting Studies and Other Quantum Mechanical Properties of 3-Phenyl-5-Isooxazolone Using Experimental and Computational Strategies. *J. Mol. Struct.* **2020**, *1203*, 127461. https://doi.org/10.1016/j.molstruc.2019.127461.
75. Alsalme, A.; Pooventhiran, T.; Al-Zaqri, N.; Rao, D. J.; Rao, S. S.; Thomas, R. Modelling the Structural and Reactivity Landscapes of Tucatinib with Special Reference to Its Wavefunction-Dependent Properties and Screening for Potential Antiviral Activity. *J. Mol. Model.* **2020**, *26*, 341. https://doi.org/10.1007/s00894-020-04603-1.
76. Sheena Mary, Y.; Ertan-Bolelli, T.; Thomas, R.; Krishnan, A. R.; Bolelli, K.; Kasap, E. N.; Onkol, T.; Yildiz, I. Quantum Mechanical Studies of Three Aromatic Halogen-Substituted Bioactive Sulfonamidobenzoxazole Compounds with Potential Light Harvesting Properties. *Polycycl. Aromat. Compd.* **2019**, *In Press*. https://doi.org/10.1080/10406638.2019.1689405.
77. Rao, D. J.; Mary, Y. S.; Mary, Y. S.; Resmi, K. S.; Thomas, R. Structure, Spectral Features, Bioactivity and Light Harvesting Properties of Methyl and Dimethyl Anthracene: Experimental and First Principle Studies. *Polycycl. Aromat. Compd.* **2019**, 1–15. https://doi.org/10.1080/10406638.2019.1709083
78. Al-Otaibi, J. S.; Mary, Y. S.; Mary, Y. S.; Thomas, R. Quantum Mechanical and Photovoltaic Studies on the Cocrystals of Hydrochlorothiazide with Isonazid and Malonamide. *J. Mol. Struct.* **2019**, *1197*, 719–726. https://doi.org/10.1016/j.molstruc.2019.07.110.
79. Thadathil, D. A.; Varghese, S.; Akshaya, K. B.; Thomas, R.; Varghese, A. An Insight into Photophysical Investigation of (E)-2-Fluoro-N'-(1-(4-Nitrophenyl)Ethylidene)Benzohydrazide through Solvatochromism Approaches and Computational Studies. *J. Fluoresc.* **2019**, *29*, 1013–1027. https://doi.org/10.1007/s10895-019-02415-y.
80. Matondo, A.; Thomas, R.; Tsalu, P. V.; Mukeba, C. T.; Mudogo, V. α-Methylation and α-Fluorination Electronic Effects on the Regioselectivity of Carbonyl Groups of Uracil by H and Triel Bonds in the Interaction of U, T and 5FU with HCl and TrH3 (Tr= B, Al). *J. Mol. Graph. Model.* **2019**, *88*, 237–246. https://doi.org/10.1016/j.jmgm.2019.02.006.
81. Thomas, R.; Mary, Y. S.; Resmi, K. S.; Narayana, B.; Sarojini, B. K.; Vijayakumar, G.; Van Alsenoy, C. Two Neoteric Pyrazole Compounds as Potential Anti-Cancer Agents: Synthesis, Electronic Structure, Physico-Chemical Properties and Docking Analysis. *J. Mol. Struct.* **2019**, *1181*, 455–466. https://doi.org/10.1016/j.molstruc.2019.01.003.
82. Sajini, T.; Thomas, R.; Mathew, B. Rational Design and Synthesis of Photo-Responsive Molecularly Imprinted Polymers for the Enantioselective Intake and Release of L-Phenylalanine Benzyl Ester on Multiwalled Carbon Nanotubes. *Polymer* **2019**, *173*, 127–140. https://doi.org/10.1016/j.polymer.2019.04.031.
83. Mary, Y. S.; Mary, Y. S.; Resmi, K. S.; Kumar, V. S.; Thomas, R.; Sureshkumar, B. Detailed Quantum Mechanical, Molecular Docking, QSAR Prediction, Photovoltaic Light Harvesting Efficiency Analysis of Benzil and Its Halogenated Analogues. *Heliyon* **2019**, *5*, e02825. https://doi.org/10.1016/j.heliyon.2019.e02825.
84. Mary, Y. S.; Mary, Y. S.; Resmi, K. S.; Thomas, R. DFT and Molecular Docking Investigations of Oxicam Derivatives. *Heliyon* **2019**, *5*, e02175. https://doi.org/10.1016/j.heliyon.2019.e02175.

Supplementary materials

Table S1. Definition of local-symmetry coordinates and the values of corresponding scale factors used to correct the B3LYP/6-31G++ (d, p)force field calculations of N-N'-dimethylethyleneurea

No.(i)	Symbol [a]	Definition[b]	Scale factors
Stretching			
1	ν C-C (Ring)	R1	0.999
2-5	ν C-N (Ring)	R2, R3, R4, R5	0.993
6-7	ν C-N sub	R6, R7	0.993
8	ν C-O	R8	0.451
9-10	ν C-H ss	(R9+R10)/ √2, (R11+R12)/ √2	0.905
11-12	ν C-H ass	(R9-R10)/ √2, (R11-R12)/ √2	0.994
13-14	νCH3ss	(R13+R14+R15), (R16+R17+R18)	0.660
15-16	ν CH3ips	(2R13-R14-R15)/ √6, (2R16-R17-R18)/ √6	0.899
17-18	ν CH3 ops	(R14-R15)/ √2, (R17-R18)/ √2	0.999
In-Plane bending			
19	βRasy	γ 19+a(γ20+ γ23)-b (γ21+ γ22)	0.998
20	βRsym	(a-b)(γ20- γ23) +(a+b) (γ21- γ22)	0.997
21-22	βCH2sc	(γ24+γ28+γ25+γ29)/2, (γ26+γ30+γ27+γ31)/2	0.865
23-24	βCH2ro	(γ24+γ28- γ25- γ29)/2, (γ26+γ30-γ27-γ31)/2	0.875
25-26	βCH2wa	(γ24-γ28+γ25-γ29)/2, (γ26-γ30+γ27-γ31)/2	0.865
27-28	βCH2tw	(γ24-γ28-γ25+γ29)/2, (γ26-γ30-γ27+γ31)/2	0.999
29-30	β(N-C)	(γ32-γ33)/√2, (γ34-γ35)/√2	0.907
31	β(N-C-O)	(γ36-γ37)/√2	0.957
32-33	βCH3sb	(-γ38- γ39- γ40+ γ44+ γ45+ γ46)/√6, (-γ41- γ42- γ43+ γ47+ γ48+ γ49)/√6	0.960
34-35	βCH3ipb	(-γ44- γ45- 2γ46)/√6, (-γ47- γ48- 2γ49)/√6	0.999
36-37	βCH3opr	(γ44+ γ45)/√6, (γ46+ γ47)/√6	0.625
38-39	βCH3ipr	(2γ38- γ39- γ40)/√6, (2γ41- γ42- γ43)/√6	0.830
40-41	βCH3opr	(γ39- γ40)/√6, (γ42- γ43)/√6	0.999
Out of plane bending			
42	ω(C-O)	ρ 50	0.995
43-44	ω(C-N)	ρ 51, ρ 52	0.995
Torsion			
45	τRasy	b(τ53+τ57)+a(τ54+τ56)+ τ55	0.987
46	τRsym	(a-b)(τ56- τ54)+(1-a) (τ57- τ53)	0.999
47-48	τN-CH3	τ60, τ61	0.850

Where a=cos1440 , b=cos720.

Abbreviations: ν, stretching; ß, in plane bending; ω, out of plane bending; τ, torsion, ss, symmetrical stretching, ass, asymmetrical stretching, sc, scissoring, wa, wagging, tw, twisting, ro, rocking, tri, trigonal deformation, sym, symmetrical deformation, asy, asymmetric deformation, sub, substitution.

a These symbols are used for description of the normal modes by PED

b The internal coordinates used here are defined in table given in supplementary material 1

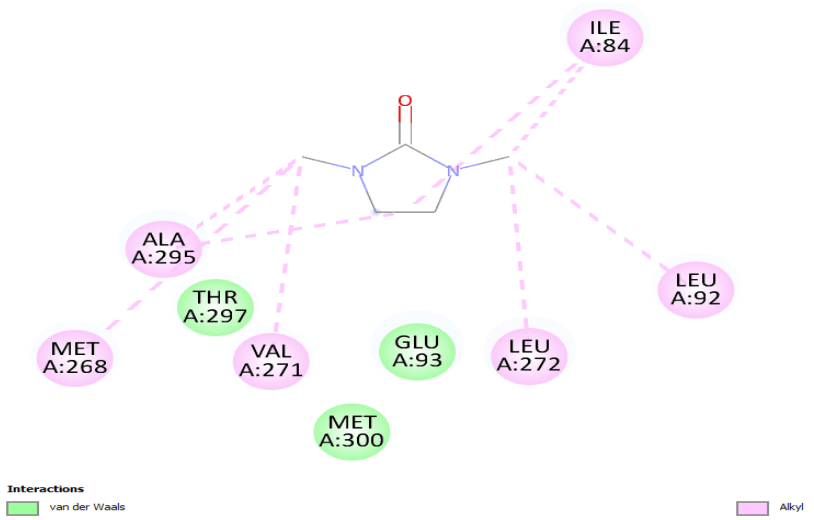

Figure S1. Hydrophobic interactions between N-N'-dimethylethylene urea and protein residues.

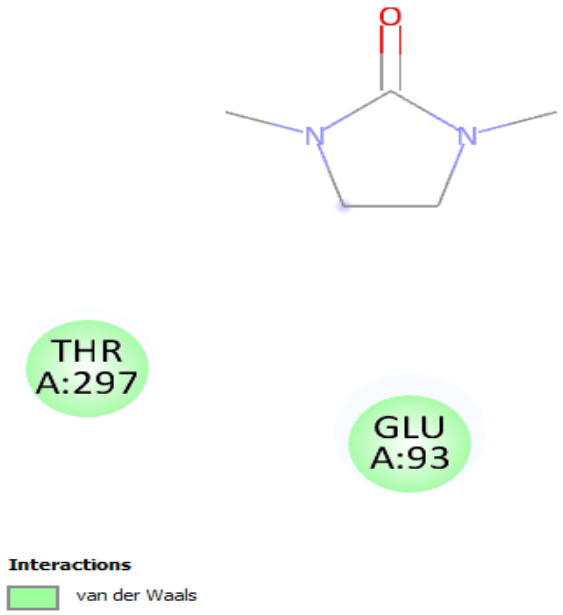

Figure S2. Hydrophilic and acid interactions between N-N'-dimethylethylene urea and protein residues.

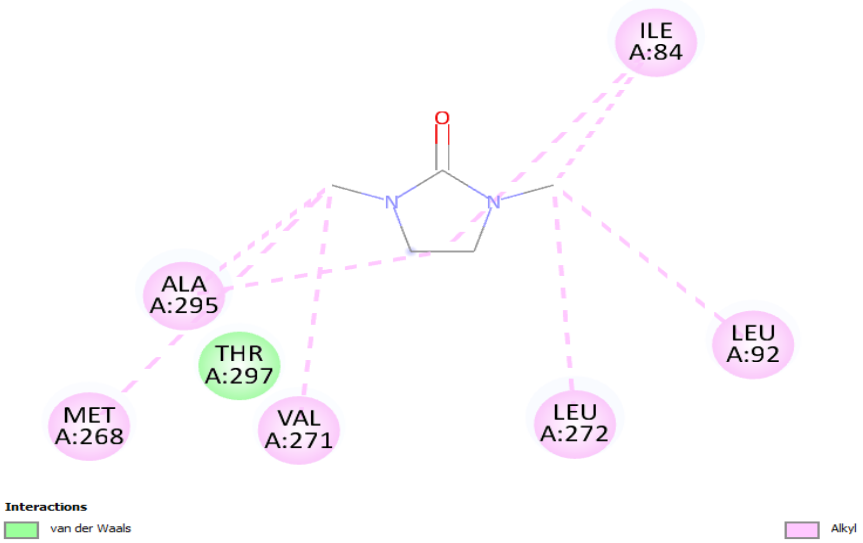

Figure S3. Neutral group interactions between N-N'-dimethylethylene urea and protein residues.